

Spectral Classification and Luminosity Function of Galaxies in the Las Campanas Redshift Survey

BENJAMIN C. BROMLEY AND WILLIAM H. PRESS,

Physics Department, Harvard University, and Harvard-Smithsonian Center for Astrophysics

HUAN LIN

Department of Astronomy, University of Toronto

and

ROBERT P. KIRSHNER

Harvard-Smithsonian Center for Astrophysics

ABSTRACT

We construct a spectral classification scheme for the galaxies of the Las Campanas Redshift Survey (LCRS) based on a principal component analysis of the measured galaxy spectra. We interpret the physical significance of the spectral classes and conclude that they are sensitive to morphological type and the amount of active star formation. In this first analysis of the LCRS to include spectral types, we find that the general luminosity function for the survey, expressed as a weighted sum of type-specific luminosity functions, exhibits a broad shoulder centered on an absolute magnitude of $M \approx -20$ in the R -band, a significant deviation from the Schechter parameterization. At fainter magnitudes, the slope of this luminosity function rises steadily; at $M = -17.5$ it has a value of $\alpha \approx -1.1$, steeper than predicted in a type-independent analysis. The luminosity functions of the individual spectral types show a smooth steepening of the faint-end slope from $\alpha \approx +0.5$ for early types to $\alpha \approx -1.9$ for late types. We also find that for a given spectral type the luminosity function can depend on environment. Specifically, the faint-end slope in the case of early-type galaxies steepens significantly with increasing local density. These results, coupled with the known density-dependence of the relative populations of galaxy types, may explain the discrepancy between the luminosity functions of the LCRS galaxies and other redshift catalogs such as the Century Survey (Geller et al. 1997). Furthermore, these results have interesting implications for theories of galaxy formation, for they suggest that galaxies of a given type are, on average, fainter when they are located in high-density regions of the Universe.

Subject headings: galaxies: luminosity function — surveys — cosmology: observations — cosmology: large-scale structure of the universe

1 Introduction

Classification of galaxies has long been regarded as an important step toward understanding galaxy formation and evolution. There is considerable evidence that the two main methods of classification—morphological and spectral—both directly reflect physical properties of galaxies (Roberts & Haynes 1994). Indeed it was clear early on that these two methods yield galaxy types which are strongly correlated (Morgan & Mayall 1957), although recent work shows that the correlation is not perfect (Connolly et al. 1995; Zaritsky, Zabludoff & Willick 1995). In preparation for large galaxy catalogs such as the Sloan Digital Sky Survey efforts have begun to automate both approaches to classification. Morphologically-based schemes must of necessity deal with pixel images, and the most promising technique employs artificial neural networks (e.g., Odewahn et al. 1996; Folkes, Lahav & Maddox 1996). Spectral schemes, on the other hand, require no more information than is already available in a typical redshift catalog. Furthermore, the interpretation of a spectral type is facilitated by the direct connection between spectral features and the physics of the stars and gas within the galaxies.

The information contained in a set of galaxy spectra can be extracted in an efficient manner by a principal component method (e.g., Connolly et al. 1995). The idea is to identify features of the spectra which show the greatest variation from galaxy to galaxy, so that a classification scheme can reflect those physical properties which maximally distinguish galaxies. We here apply the principal component method to analyze the galaxies in the Las Campanas Redshift Survey, a large multiple-strip survey with over 25,000 measured spectra.

The goal of the work described here is not only to define spectral types but to determine general physical properties of the galaxies in each type. We focus on the luminosity function, an important constraint for models of cosmic structure formation. The large size of the LCRS catalog allows us to address questions such as the dependence of luminosity on galaxy type, and whether the luminosity function is universal, that is, whether it depends on local density or other environmental effects.

In this paper we first review parameters of the LCRS catalog (§2). Then, in Section 3, we outline the principal component method and compare our classification scheme with previous work. In Section 3 we analyze luminosity functions of the galaxies according to spectral type, and estimate the type-dependence of measures of clustering. We close with a discussion of the implications of our findings.

2 The Redshift Data

The Las Campanas Redshift Survey is described in detail in Shectman et al. (1996; hereafter LC1). Lin et al. (1996; hereafter LC2) provide additional details related to galaxy selection. We summarize characteristics of the survey briefly in this section.

The survey consists of $\sim 26,000$ galaxies in six sky strips, three strips in the northern Galactic cap region and three in the southern region. Each strip runs approximately 80° across the sky in right ascension and has a width in declination of $\sim 1.5^\circ$. The mean strip declinations are -3° , -6° and -12° in the northern sample and -39° , -42° and -45° in the south.

Each sky strip was subdivided into 50 or so fields of square or nearly square dimensions. Galaxies in each field were selected on the basis of Kron-Cousins R -band magnitudes; a subset of these galaxies were chosen randomly for spectroscopic study using multiobject fiber spectrometers of either 50 or 112 fibers. Apparent magnitude limits vary from field to field, with typical isophotal limits of $16.0 \leq m < 17.3$ and $15.0 \leq m < 17.7$ for the 50-fiber and 112-fiber fields, respectively. Additional limits were imposed on the basis of “central surface brightness” of the galaxies, corresponding approximately to the flux entering a fixed fiber aperture of $3.5''$. This additional cut amounts to a 20% reduction in the fraction of galaxies in the 50-fiber fields and less than a 10% reduction of the 112-fiber fields. We emphasize that each field has assigned to it a unique set of parameters which include isophotal magnitude limits, central magnitude cut, and “sample fraction” of the total galaxies in that field for which spectra were observed. As in LC2, we take full account of these field-to-field differences.

While we work with the full catalog to perform the spectral classification in the next section, our analysis in §4 of the luminosity function makes use of a subset of galaxies, as in LC2. Specifically we consider only galaxies with redshifts below $cz = 60,000$ km/s and with absolute magnitudes between -23 and -17.5 . We also largely exclude the 50-fiber data because of their more stringent surface brightness cuts. This leaves 18,098 objects, 8643 in the north and 9462 in the south. Where we use the 50-fiber data, we have an additional 2665 and 1980 objects in the north and south, respectively, for a total of 22,743 galaxies. We adopt the same labeling scheme as in LC2 so, for example, N112 refers to the northern 112-fiber data.

3 Spectral Classification

Toward quantitative classification of the LCRS catalog we seek a representation of the spectra which accentuates the differences between individual galaxies. Such a representation is afforded by singular-value decomposition (SVD) as part of a principal component analysis (see Kendall 1975). The overall strategy is to express the spectra in terms of a series of templates—following Connolly et al. (1995) we call them “eigenspectra”—and to select those which are most sensitive to galaxy-to-galaxy variations. The coefficient obtained by projecting a galaxy’s spectrum onto such an eigenspectrum can serve as its spectral type. Singular-value decomposition gives the general prescription for how to build the eigenspectra; principal component analysis demonstrates that they indeed characterize those properties of the galaxies which optimally distinguishes them.

3.1 Singular-value decomposition

Let the vector s_i represent the spectrum of the i^{th} galaxy in a catalog of N objects. The components of the vector, s_{ij} , are integrated fluxes in frequency channels, where j is the channel index. The full catalog then

is a matrix S of size $N \times M$ where N is 25,327 and the number of channels, M , is 800. We are interested here in the intrinsic differences between galaxies, so we preprocess the data first by shifting all spectra in the original catalog to the rest frame. We then normalize the spectra to some constant flux value in the wavelength range of 3500 Å to 5000 Å, and determine the mean spectrum by averaging the flux in each frequency bin over all spectra in the catalog. Next we subtract off the catalog mean—we want the power in the eigenspectra to reflect differences between galaxies, not their similarities. It is this shifted, normalized, zero-mean entity which we call the catalog, S .

We can write the matrix S in the form

$$S = UWV^T, \quad (1)$$

where U is a row-orthogonal $M \times N$ matrix, and W and V are both $M \times M$; the former is diagonal with elements $w_i \geq 0$ and the latter is orthonormal (cf. Press et al. 1992, §2.6). This equation is the singular-value decomposition of S . It is generally valid for all matrices provided that the number of columns does not exceed the number of rows, i.e., $N \geq M$.

Notice that any single spectrum \mathbf{s}_i from the catalog can be easily reconstructed from the matrices U , W and V in equation (1):

$$\mathbf{s}_i = \sum_{j=1}^M \gamma_{ij} \mathbf{v}_j \quad (2)$$

where γ_{ij} is the ij^{th} element of the product UW , and the vector \mathbf{v}_j is the j^{th} column of V . This property highlights the special significance of V : its columns define orthonormal vectors $\mathbf{v}_1 \dots \mathbf{v}_M$, the eigenspectra which form the basis used in a principal component analysis. The defining characteristic of such a basis is that it diagonalizes the covariance matrix of the catalog,

$$\begin{aligned} C &\equiv S^T S, \\ &= VW^T U^T UWV^T, \\ &= VW^2 V^T, \end{aligned} \quad (3)$$

(note that $U^T = U^{-1}$). Projecting the expressions in equation (3) onto the eigenspectra explicitly demonstrates that C is diagonalized, leaving the eigenvalue equation

$$C\mathbf{v}_i = w_i^2 \mathbf{v}_i, \quad (4)$$

where w_i is the i^{th} diagonal element of W in equation (1).

There may also be value in weighting individual data points differently, depending on measurement errors or prior assumptions about the data. Thus, before calculating the SVD, one may wish to write the elements of the catalog matrix as

$$s_{ij} \rightarrow g_i h_j s_{ij}, \quad (5)$$

where g_i and h_j are weight factors. In this paper we do an initial “flattening” and renormalization of the spectra, which can be viewed as a transformation of this type.

A geometric interpretation of the eigenspectra is that they are aligned with the principle axes of the error ellipsoid corresponding to the scatter of points in the catalog. The eigenspectra with the largest eigenvalues (the w_i^2 in eq. [4]) indicate directions in the space of frequency channels where there is greatest variation between objects in the catalog. Conversely, small eigenvalues correspond to directions along which the data show little variation.

The idealization that data scatter is an error ellipsoid hints that a principal component analysis is best suited to systems where the data correspond to M statistically independent Gaussian variates. Knowledge of the covariance matrix allows the original orthogonal basis in which the data are collected (e.i., frequency channels) to be rotated into a new basis (the eigenspectra) to represent the data in terms of statistically independent coefficients (the γ_{ij} in eq. [2]). This rotation is the Karhunen-Loëve transform. In general, where higher-order correlations are possible, these coefficients will not necessarily be statistically independent.

A data compression algorithm is evident from the geometrical interpretation above: Simply keep only the first m eigenspectra \mathbf{v}_j and coefficients γ_{ij} which correspond to eigenvalues at or above a threshold w_m^2 ; all the rest correspond to modes along which the data show relatively small variation. Our galaxy classification method follows just this strategy.

The simplest scheme is to consider only γ_{i1} , the dot product of the i^{th} galaxy spectrum with the first eigenspectrum \mathbf{v}_1 . The galaxies have the greatest variance with this coefficient and it alone may be sufficient to usefully define spectral type. Then the values of γ_{i1} could be partitioned into bins, with each bin corresponding to a unique type. Here, we use the first two eigenspectra (Figure 1) to define spectral type because the symmetry of data-point scatter in the vector space of frequency channels is not exactly elliptical; there exist correlations between coefficients such that the scatter of data points roughly forms an arc. We create distinct types by extending boundaries radially outward from a point at some distance from the arc. Figure 2 illustrates the six spectral types — here called “clans” — defined in this way.

Before analyzing astrophysical properties of the clan populations, we discuss qualitatively the line and continuum features which appear in the eigenspectra. This will help place our classification scheme in the context of morphological classification and other spectral classification methods.

3.2 Physical Significance of the Eigenspectra

Recall that in deriving the eigenspectra, we subtract the mean spectrum of the 25,327 galaxies. Thus the eigenspectra measure differential signal in continuum and line features. Figure 1 contains the mean spectrum of the LCRS galaxies along with the first four eigenspectra. The first eigenspectrum shows emission features in H I, He I, O II, O III, Ne III, Ca (H & K) and Mg I, as well as slight continuum “absorption” on the red side of the 4,000Å Balmer limit. Because the individual spectra are high-pass filtered, i.e., flattened, the 4,000Å break shows up as sawtooth-shaped profile. Some of the emission features—H β and forbidden O II and O III lines—are direct indicators of physical processes, presumably in the interstellar medium. Others, such as the Ca H & K lines and G-band complex lines, appear in “emission” primarily to compensate for spectra with weaker absorption than is exhibited in the mean spectrum.

Evidently, the most significant spectral variation between galaxies is the degree of line emission. Emission lines of oxygen and hydrogen Balmer lines are expected from H II regions, while the diminished stellar absorption in the calcium lines indicate a young stellar population. Therefore a positive projection coefficient from this eigenspectrum seems like a good indicator of star formation. Indeed, the most prominent feature in the eigenspectrum, the [O II] $\lambda 3727$ line, is known to correlate with star-formation rate as well as morphological type (Kennicutt 1992a). However, there are two caveats. The first is that better measures of star formation are known, specifically $H\alpha$ flux and the shape of the UV continuum, but both are outside of the waveband considered here. The second caveat is that it can be difficult to make a distinction between star-forming regions and AGNs or LINERs solely on the basis of the emission lines contained in the eigenspectrum. Again, $H\alpha$ measurements would have helped (Baldwin, Phillips & Terlevich 1981; Allen et al. 1991). The fraction of objects with non-thermal spectra is expected to be small and therefore we hold to the interpretation that emission lines associated with the first eigenspectrum indicate star formation. Below we present evidence (Fig. 4) that AGN spectra can be isolated, but using the coupling coefficient with the third eigenspectrum.

The second eigenspectrum is primarily dominated by [O II] (3727 Å), [O III] (5007 Å), and H γ (4340 Å) emission lines. It allows a fine-tuning of the line contributions in star-forming galaxies—there is tendency for galaxy spectra which are strongly coupled to the first eigenspectrum to show strong coupling with the second eigenspectrum as well. This correlation is manifested by the curvature of the data scatter in Figure 2. The appearance of strong H δ emission in the eigenspectrum suggests that it positively correlates with strong star formation H II regions at relatively high levels of excitation.

Ultimately, the physical significance of the eigenspectra is best interpreted by examining the spectra which they represent. In Figure 3 we show the average spectra of objects in the six clans. A progression from clan to clan is clear and supports our interpretation that the most important spectral differences between galaxies lie in the amount of line emission. This is in agreement with the recent findings of Kurtz & Mink (1997) from their catalog of $\sim 2,000$ R -band selected objects.

While not relevant to our present spectral classification scheme, the third eigenspectrum is noteworthy. It has the role of further fine-tuning specific line-emission features including [O III] $\lambda 3727$, as well as continuum emission above 4000 Å. Note that it shows strong absorption in H γ and H δ and an asymmetry in the Ca H&K troughs from He. The distribution of projection coefficients for this eigenspectrum is roughly symmetric except for a weak tail extending to large negative values, with a significant population—about 0.6% of the total—between three and seven standard deviations. The mean spectrum of these objects is shown in Figure 4. The coupling with the third eigenspectrum is negative for this population, hence it shows strong emission in the Balmer series. With the pronounced, broad Balmer lines and enhanced [O III]/O[II], we interpret these objects as Seyfert 1 galaxies (cf. Kennicutt 1992b).

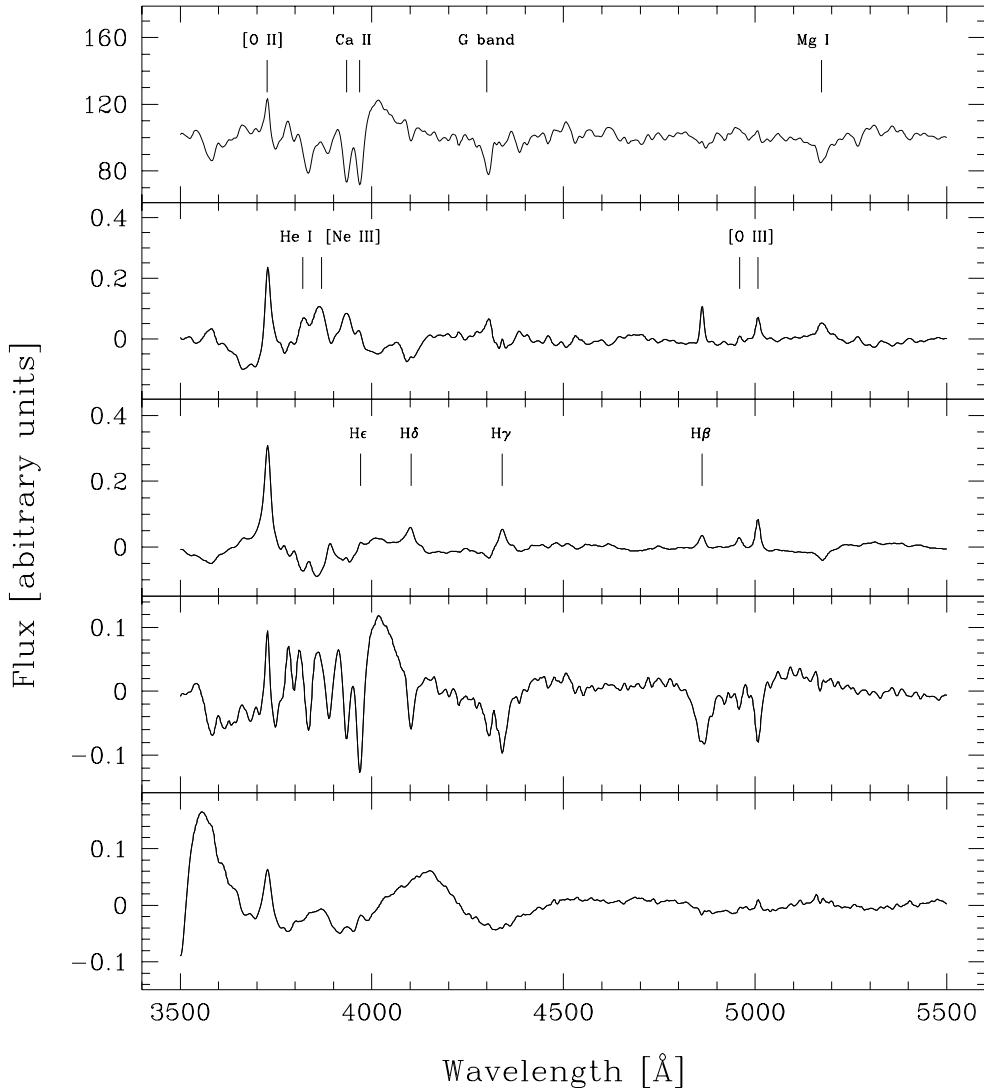


Fig. 1.—The mean spectrum of the LCRS galaxies after high-pass filtering (top), and the first four eigenspectra from singular-value decomposition. The first eigenspectrum (which has the largest eigenvalue) is second from the top, the second eigenspectrum is immediately below it, and so forth. The wavelength of some atomic line features are marked; note that these features represent either emission or absorption, depending on the sign of the weight factor multiplying each eigenspectrum.

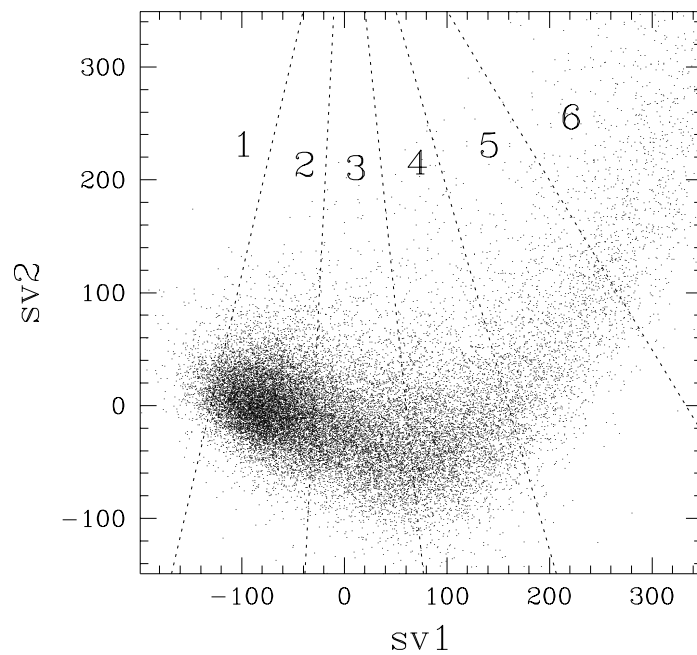


Fig. 2.— Scatter diagrams of the projection coefficients (sv1 and sv2) for the first and second eigenspectra in Figure 1. The regions determined by the straight lines define the galaxy clans, labeled 1 through 6.

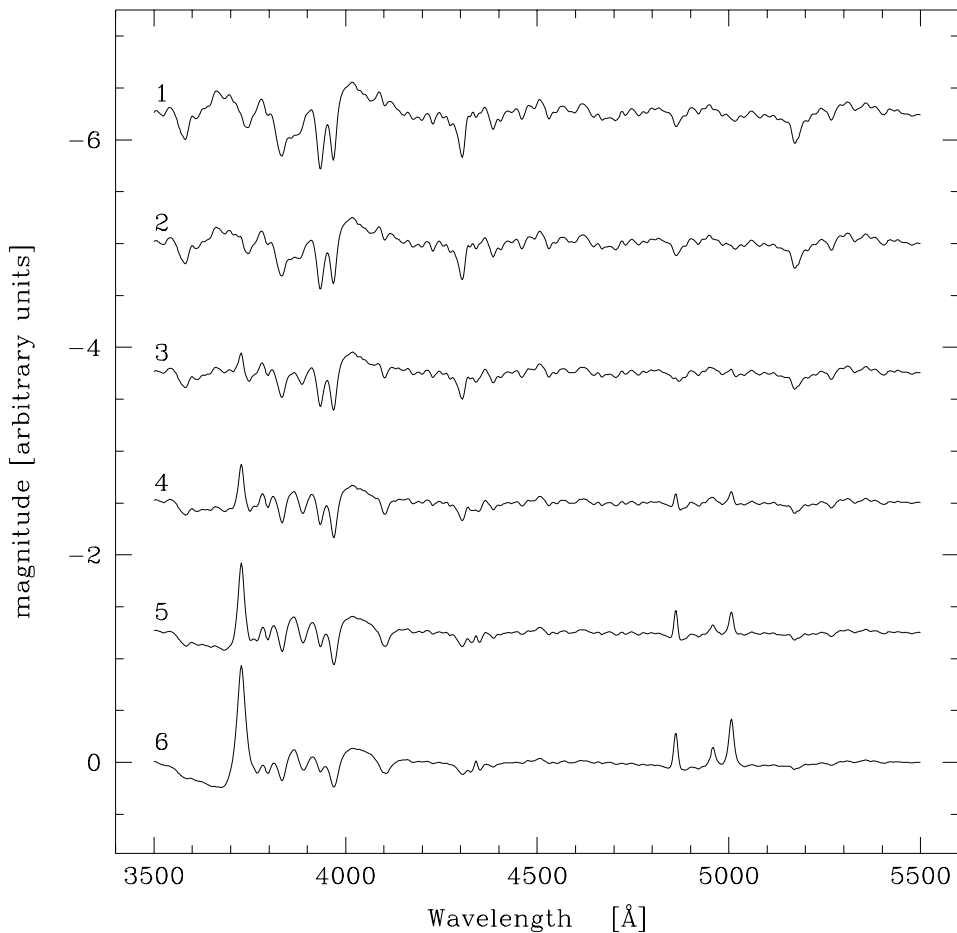


Fig. 3.— The mean spectra of the six clans. A low-frequency component has been removed, as in Figure 1, and each curve has been offset for clarity. The labels indicate the clans as defined in Figure 2.

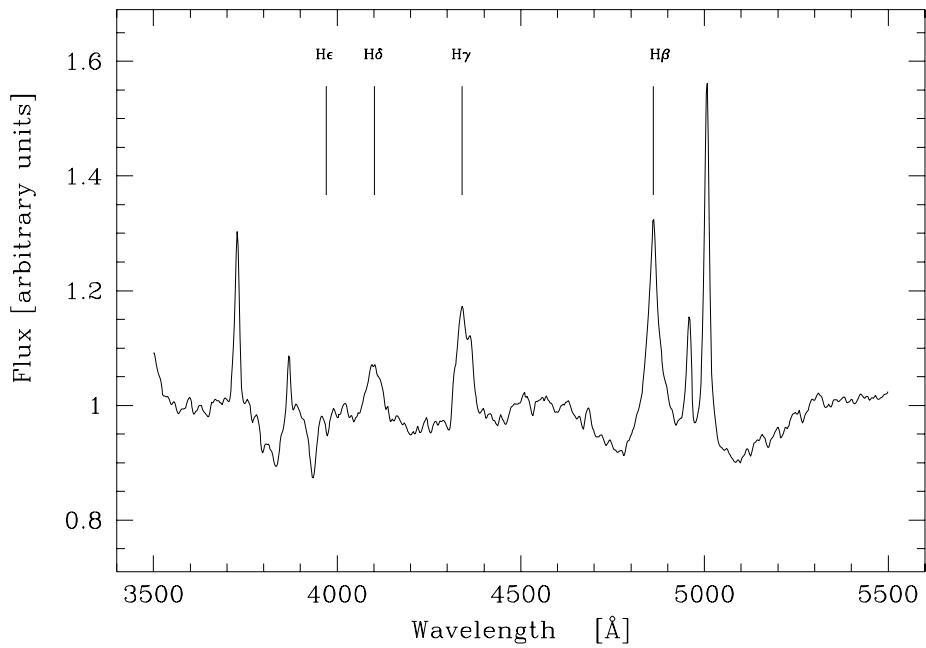


Fig. 4.— The mean spectrum of galaxies with abnormally strong, negative projection coefficients for the third eigenspectrum. As in Figure 3, the a low-frequency component has been removed. Strong Balmer emission is evident in the spectrum, and the interpretation here is that these are Seyfert 1 galaxies.

The skewness in the distribution of projection coefficients steadily decreases with increasing eigenspectrum index. By the fourth eigenspectrum, the distribution is nearly symmetric (skewness is around 0.2, as compared with 1.2 for the first eigenspectrum). This is reassuring because it suggests that the scatter in the higher-order eigenspectra is becoming more and more characteristic of Gaussian scatter, and contains less information relevant to classification.

3.3 Comparison with other Spectral Classification Schemes

A variety of spectral classification schemes for galaxies has been proposed in the literature, and recent examples include Allen et al. (1991), Bershady (1995), Zaritsky, Zabludoff & Willick (1995) and Kurtz & Mink (1997). Most of these methods involve fitting to specific line features or to a predefined spectral template which includes these features. Connolly et al. (1995) proposed a method which incorporates eigenspectra defined primarily from the data itself in a strategy very similar to the one used here. We begin this section by considering their technique.

Connolly et al. performed a principal component analysis of optical and UV data to classify galaxies according to the projection of their spectra onto eigenspectra. The eigenspectra were derived from a set of 10 templates, where each template is the average of spectra for a given morphological type or class of starburst galaxy. Since the number of frequency channels is large, over 2200 in their case, Connolly et al. properly construct their correlation matrix using the space defined by the 10 templates, not the space of frequency channels. Thus each “data point” is essentially a measure of how the flux is distributed among the 10 templates. Connolly et al. also assign a variable weight to each template (as in eq. [5]), but otherwise, the procedure is the same as in a “standard” principal component analysis. Connolly et al. argue that their projection of the data onto the space of templates offers several advantages over the standard method, not the least of which is a reduction in computational load. In general, there is considerable savings in diagonalizing a 10×10 matrix versus one of size 2200×2200 (although of rank 10).

A nice way to view the differences between the method of Connolly et al. and a standard principal component analysis is through the formalism of SVD. The raw data, in this case a 10×2200 matrix formed of 10 vectors in the 2200-dimensional space of frequency channels, is projected onto the 10-dimensional space of templates simply with a matrix transpose operator. Indeed, it is formally necessary to take the transpose of equation (1) to interpret the matrices V and W in terms of eigenspectra and eigenvalues as we did earlier—this enables the data of Connolly et al. to meet the requirement that the number of rows is greater than the number of columns. Numerically, it is not at all necessary to work with the transpose. One simply performs the SVD and pulls the eigenspectra out from the rows of the matrix U in equation (1) (see Press et al. 1992, p. 66).

In practice it may not be feasible to work with a SVD algorithm if the number of data points and the number of frequency channels are large compared with available machine memory. Instead, one may calculate and diagonalize the covariance matrix directly without ever forming the catalog matrix. For this purpose we still recommend an SVD algorithm.

Once the eigenspectra were defined, Connolly et al. projected individual galaxy spectra onto them; a classification scheme based on projection coefficients for the first two eigenspectra produced a spectral type that was strongly, but not perfectly, correlated with morphology. It should be noted that the eigenspectra are most responsive to continuum emission, particularly to that on the blue side of the 4000 Å break.

In contrast Zaritsky, Zabludoff & Willick (1995) focussed on line features. They defined a 3-dimensional space based on ratios of line emission and absorption, projection onto stellar templates of young (spectral class A) and old (K) stars, and ratio of hydrogen to oxygen emission lines. A “training set” of spectra enabled the authors to determine the loci of points in this space which correspond to morphological types. They tested the distance from these loci as measures of type using an independent set of galaxy spectra, and they concur with Connolly et al. that the correlation between spectral and morphological types is strong but not perfect. Like Connolly et al., Zaritsky et al. make the important point that the lack of perfect correlation is not the result of flaws in the spectral classification scheme, but rather reflects an intrinsic property of galaxies.

The spectral classification scheme presented here is considerably more sensitive to spectral features than to the shape of the continuum, hence, it is qualitatively similar to the method of Zaritsky et al. Indeed, two of their parameters have direct correspondence to the eigenspectra presented here: the first eigenspectrum is sensitive to the ratio of absorption to emission features, while the second is responsive to changes in the hydrogen to oxygen emission. The third parameter used by Zaritsky et al., a combination of coupling

coefficients with A-star and K-star templates, evidently has relatively small galaxy-to-galaxy variance (Fig. 3 therein)—this parameter is not highly effective as a type-discriminator.

The classification scheme presented here differs in an important way from the methods of both Connolly et al. and Zaritsky et al. In the previous work, prior knowledge of morphological class was used to define spectral types. Here, we adopt a classification scheme using spectral characteristics which have maximal variation among catalog members, irrespective of other galaxy properties. A limitation is that the scheme will have some dependence on survey selection criteria. A benefit is that the resulting classes will automatically quantify the most outstanding differences between spectra of a catalog, no matter what the survey selection, instrumental response, or whether the physical processes which generate these differences are known.

Kurtz & Mink (1997) devised a classification scheme which is based on direct estimates of the effects of survey selection, instrumental response and the astrophysics of line formation to model template spectra without recourse to a statistical approach such as the method used here. They found that their data could be described simply and accurately by a linear combination of an absorption spectrum and an emission spectrum, with the following physical interpretation: All galaxies exhibit the absorption spectrum generated by their constituent stellar populations, but many also have superimposed emission features from physically distinct H II regions. Thus spectral classes may be derived simply from the degree of coupling with the emission-line template. Interestingly, a large fraction of the $\sim 2,000$ galaxies in their survey cluster do not couple appreciably with this template. The peak in the distribution of projection coefficients for our first eigenspectrum reflects just this behavior, although in Figure 2 a fair amount of scatter is evident about the peak. One can ask whether our “clan-1” galaxies, a small population with absorption-dominated spectra, represent random scatter among the bulk of galaxies which have no line emission or whether they are intrinsically different. We find below evidence that the galaxies have physically distinct properties (Table 1).

Given the similarities between our classification scheme and those for which morphological types have been considered, it is likely that the clans and morphological type are strongly correlated. Thus we adopt the nomenclature of “early” and “late” types to refer to galaxies solely on the basis of clan membership, with low clan number corresponding to early types. We now proceed to consider the clan-dependence of galaxy properties; we keep our focus primarily on the luminosity function.

4 Luminosity Functions

In their comprehensive review, Binggeli, Sandage & Tammann (1988) point out that the luminosity function of galaxies Φ , giving the distribution of galaxies as a function of absolute magnitude M , should be defined in terms of galaxy types. They argue, as have others (Holmberg 1958 seems to be the first), that galaxies of different morphological type have different luminosity functions. Thus, we write the general luminosity function of the full LCRS catalog to be

$$\Phi_g(M) = \sum_{c=1}^6 f_c \Phi_c(M) , \quad (6)$$

where Φ_c is the luminosity function for the c^{th} clan, and f_c is the fraction of all galaxies of the c^{th} clan in some specified region of the Universe. Here we treat all luminosity functions as probability distributions, hence Φ_g and the Φ_c are normalized to unity upon integration over all absolute magnitude values in the range of interest:

$$\int_{M_{\text{bri}}}^{M_{\text{dim}}} dM \Phi(M) = 1 ; \quad (7)$$

In our analysis $M_{\text{dim}} = -17.5$ and $M_{\text{bri}} = -23.0$.

In principle, there can exist a universal luminosity function that applies to all galaxies without any dependence on local environment. A case can be made against universality, and we attempt to strengthen it here. Binggeli et al. provide the starting point, the assumption that while the general luminosity function is not universal, the luminosity functions of the individual clans are. Then, one can argue against universality if the clan luminosity functions differ from one another and if the relative clan population depends on local density as is anticipated (Dressler 1980). An implausible conspiracy would be required to maintain universality when the luminosity function and local density both vary with galaxy type. As a first application of the

spectral classification scheme presented here, we address these issues of type dependence and universality. We begin with an outline of our methodology.

4.1 Method of Estimation

We estimate luminosity functions for the LCRS galaxies using a procedure which is almost identical to that described in LC2. First, we apply the non-parametric estimator proposed by Efstathiou, Ellis & Peterson (1988) to obtain the unconstrained form of the luminosity functions. Then we fit the data with Schechter functions,

$$\Phi(M) = C 10^{-0.4(\alpha+1)(M_* - M)} \exp(-10^{0.4(M_* - M)}) , \quad (8)$$

where α and M_* correspond to the slope of the faint-end of the galaxy distribution and to a typical absolute magnitude, respectively, and C is a normalization constant,

$$C = \frac{1}{\Gamma(\alpha + 1, 10^{-0.4(M_* - M)})} \bigg|_{M=M_{\text{bri}}}^{M_{\text{dim}}} . \quad (9)$$

Note that absolute magnitudes are calculated on the basis of relativistic luminosity distances with cosmological deceleration parameter $q_0 = 0.2$ and Hubble parameter $H_0 = 100 \text{ km/s/Mpc}$. As in LC2, the results presented here are insensitive to the choice of q_0 in the range of 0.1 to 0.5; the specification of the Hubble parameter is necessary only to relate absolute magnitudes to physical luminosities.

In addition to fitting the luminosity function with a parametrized form, we assess its “natural” shape with a nonparametric method. The nonparametric representation of choice is a step-wise function (first-order spline or histogram) of constant bin width δM in magnitude:

$$\Phi(M) \approx \sum_{n=-\infty}^{\infty} \phi_n W_{TH}(M - n\delta M) , \quad (10)$$

where ϕ_n are constants, and W_{TH} is a tophat function of unit height and width, centered at the origin. Of course we cut the summation so that $n\delta M$ lies between M_{bri} and M_{dim} , but even so, “nonparametric” evidently implies a large number of parameters.

The weights ϕ_i in equation (10)—or the parameters of any model of a luminosity function—can be determined from a maximum likelihood analysis (Sandage, Tammann & Yahil 1978). Define p_i to be the probability of observing the i^{th} galaxy in a catalog with an absolute magnitude M_i , given that it is located at some specified redshift. This is equivalent to the fraction of such galaxies that could be observed given the catalog’s minimum and maximum apparent magnitude cuts and other selection criteria. The likelihood that the full catalog of galaxies was observed, given their redshifts, absolute magnitudes, the survey window, is just the product

$$\mathcal{L} = \prod_{i=1}^N p_i . \quad (11)$$

The form of the luminosity function can be estimated by first guessing it and then functionally deforming it to maximize the likelihood function in equation (11). If the number of parameters needed to determine the luminosity function’s form is small, then a direct search of the parameter space quickly yields the best-fit. Otherwise, as in the case of the nonparametric luminosity function in equation (10), the best fit can be obtained from iterative corrections using constraints from the derivative of \mathcal{L} with respect to the ϕ_i . Uncertainties in the best-fit luminosity function are calculated either by directly mapping relative confidence levels from the likelihood function or by calculating elements of the covariance matrix. Again, see Efstathiou et al. or LC2 for details.

One virtue of the maximum-likelihood method is that it is insensitive to the density field—the probability p_i represents the *fraction* of galaxies observable at a given magnitude and this quantity is independent of density as long as the luminosity function itself is not density-dependent. We are assuming for the moment that this is true, at least for the clan luminosity functions.

To complete the estimation of the general luminosity in equation (6), we need the number density of galaxies in each clan. Since density factors out of the maximum-likelihood estimators, it must be estimated

Table 1: Luminosity function parameters by clan

Clan	N	α	M_*	$\bar{n} \times 10^{-3} \text{ h}^3 \text{Mpc}^{-3}$	f_{high}^1
1	655	0.51 ± 0.14	-20.29 ± 0.07	0.35 ± 0.02	52.2%
2	7596	-0.12 ± 0.05	-20.23 ± 0.03	6.7 ± 0.5	40.7
3	4653	-0.31 ± 0.07	-19.89 ± 0.04	8.6 ± 0.1	35.2
4	3190	-0.65 ± 0.08	-19.86 ± 0.05	9.1 ± 0.2	30.0
5	1393	-1.23 ± 0.10	-19.95 ± 0.09	4.5 ± 1.3	30.0
6	618	-1.93 ± 0.13	-20.10 ± 0.16	5.1 ± 3.4	23.9

¹fraction of objects in each clan which are associated with high density regions (see text).

independently. We use the same prescription as in LC2 to get the mean number density:

$$n = \frac{1}{V} \sum_{i=1}^N \frac{W_i}{\int_{M_-}^{M_+} dM \Phi(M)} , \quad (12)$$

where V is the proper volume of the survey, the integral gives the luminosity selection function, and W_i is a weight factor to account for surface-brightness selection effects and variable sampling rates in the LCRS fields (see LC2, §3.1 therein). The limits of integration in equation (12), M_{\pm} , give absolute magnitude cuts which simultaneously satisfy both the apparent and absolute magnitude limits of the survey.

4.2 Luminosity functions by clan

We apply the above procedure to the 6 clans and to the total population of the LCRS catalog observed with the 112-fiber spectrometers (NS112); the results are summarized in Figure 5, Figure 6 and Table 1. There is a clear, systematic steepening of the faint-end slope as the galaxy type progresses from early to late. The Schechter parameterization is reasonable over most of the magnitude range considered here, although the best-fit bright-end falloff may be too steep for late-type galaxies. Given that the eigenspectra used in our classification measures line emission, the trend in the faint-end slope was anticipated in LC2 from analysis of two subsets of galaxies partitioned according to the degree of O II line emission.

The clans are defined on the basis of the first two eigenspectra, as described in §3.1, but the first eigenspectrum alone may yield a reasonable classification of the LCRS galaxies. We check this possibility by rebinning the clan populations on the basis of sorted projection coefficients for the first eigenspectrum: the rebinned populations—each defined to have the same number of objects as the original clan—show slightly less clan-to-clan variation in faint-end slope. The extreme early-type galaxies are most sensitive to the rebinning, with $\alpha = 0.32 \pm 0.12$ for rebinned clan-1 galaxies, down from 0.51 ± 0.14 . The intermediate-to-late-type galaxies have luminosity functions which are only marginally affected by the rebinning. This result suggests that our analysis is not highly sensitive to the precise clan definitions. Still, there is enough information in the second eigenspectrum to justify incorporating it into the classification scheme.

The unreasonable effectiveness of the Schechter parameterization tempts us to fit not only the clan luminosity functions but the universal luminosity function for the whole catalog as well. Figure 7 compares the best-fit universal luminosity function from LC2 with a weighted sum of fitted clan luminosity functions, as in equation (6). Note that the faint-end slope of the LC2 fit is relatively flat, with $\alpha \sim -0.7$. In contrast, the faint-end slope of the weighted sum is formally $\alpha \sim -1.9$, which corresponds to the very late-type galaxies of the 6th clan. If one were to pull the faint-end slope from the behavior of the weighted sum in the range -18.5 to -17.5 Mag, then the slope would be approximately -1.1 , a value which is more in line with other redshift surveys (e.g., Marzke et al. 1994). We consider the differences between the luminosity functions of the LCRS and other surveys in more detail below (§4.4).

A refinement of the analysis that considers northern and southern populations separately preserves the general trend of faint-end slope with galaxy type. However, some of the clans, in particular clans 1 and 3, show significant differences in the northern and southern subsamples. A similar situation is discussed in LC2 for the estimation of a universal luminosity function from the full NS112 data: the error ellipsoids in the α - M_* plane overlap only at the 2σ level. A variety of effects were considered and no single explanation was

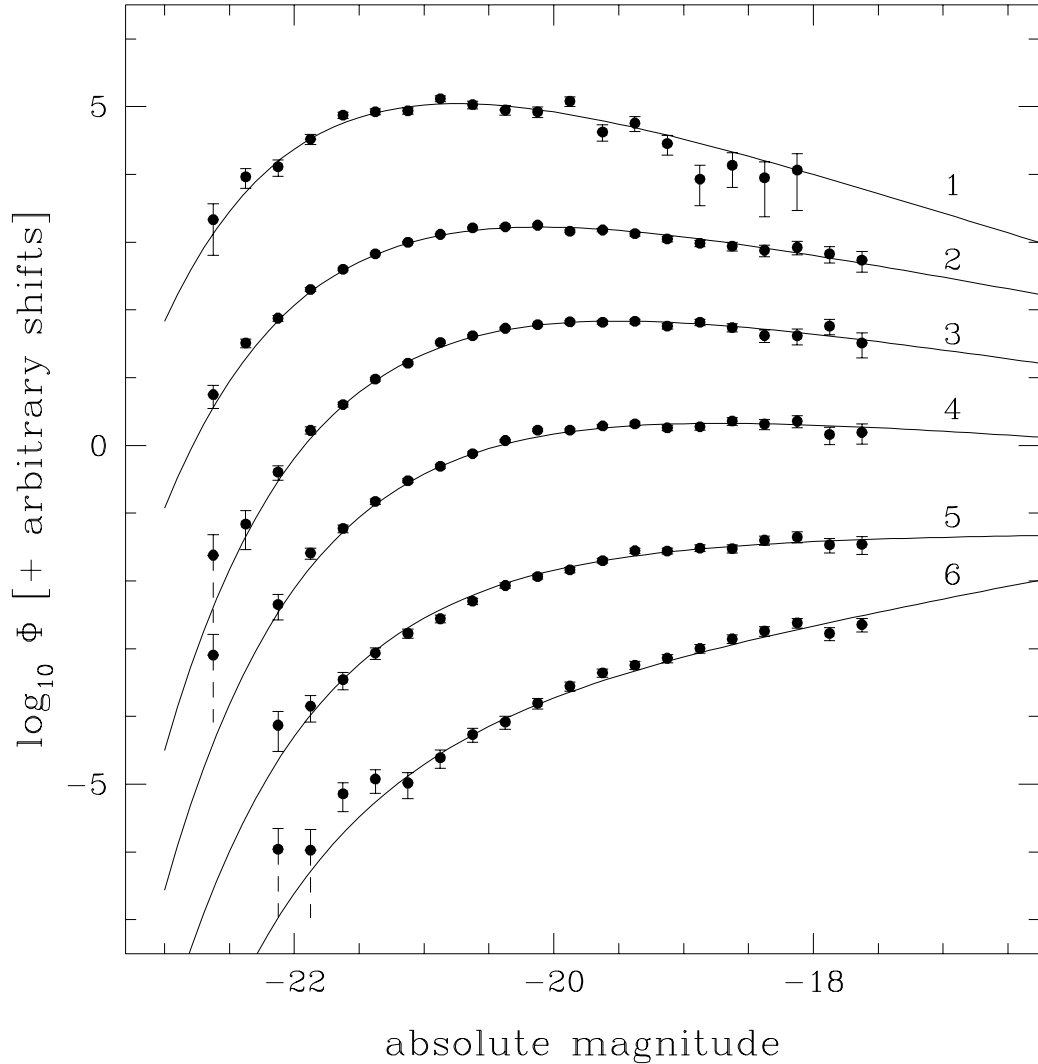


Fig. 5.— The luminosity function by clan. The points give the luminosity function from the nonparametric fit and the curves are the best-fit Schechter functions. The points and curves have been offset in the vertical direction for clarity; the labels indicate the clan identity. Error bars show $1-\sigma$ confidence limits except in cases (signified with dotted line segments) where the lower limits are formally negative.

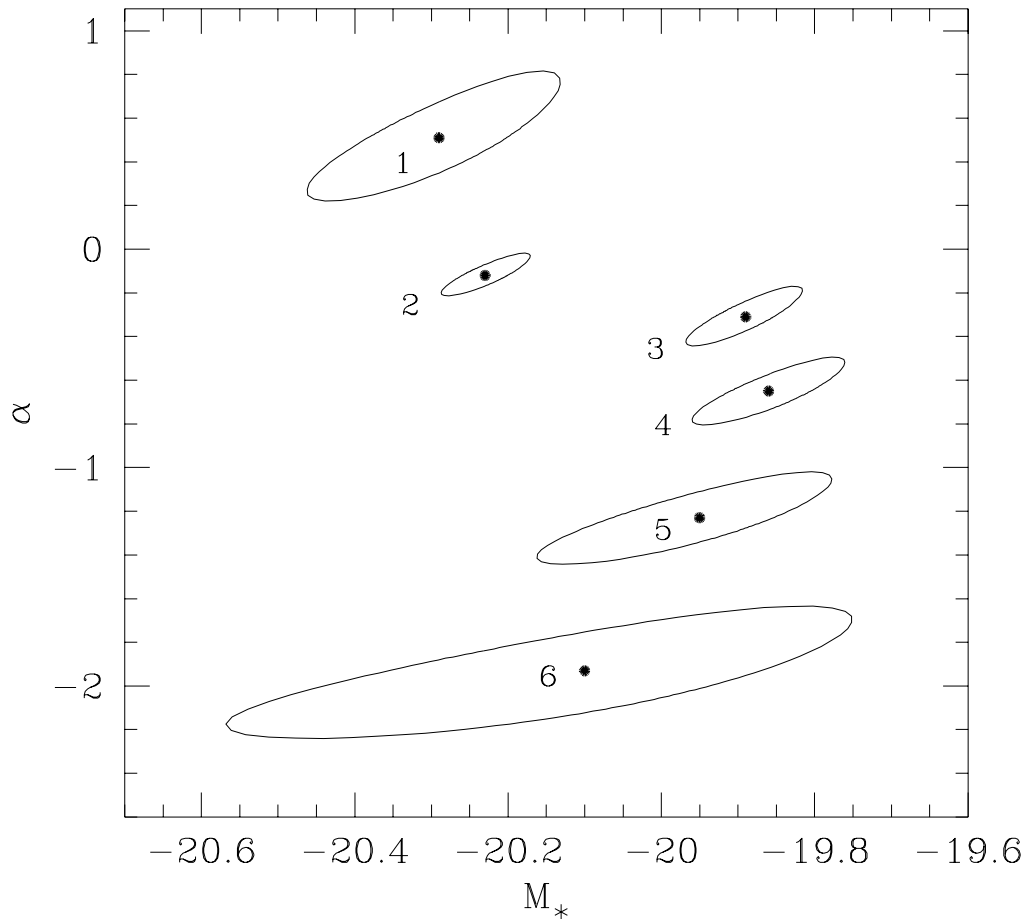


Fig. 6.—Error ellipsoids for the best-fit Schechter parameters. The labels indicate clan index, the best-fit values of M_* and α are marked with solid circle, and the ellipsoids show 95% confidence intervals.

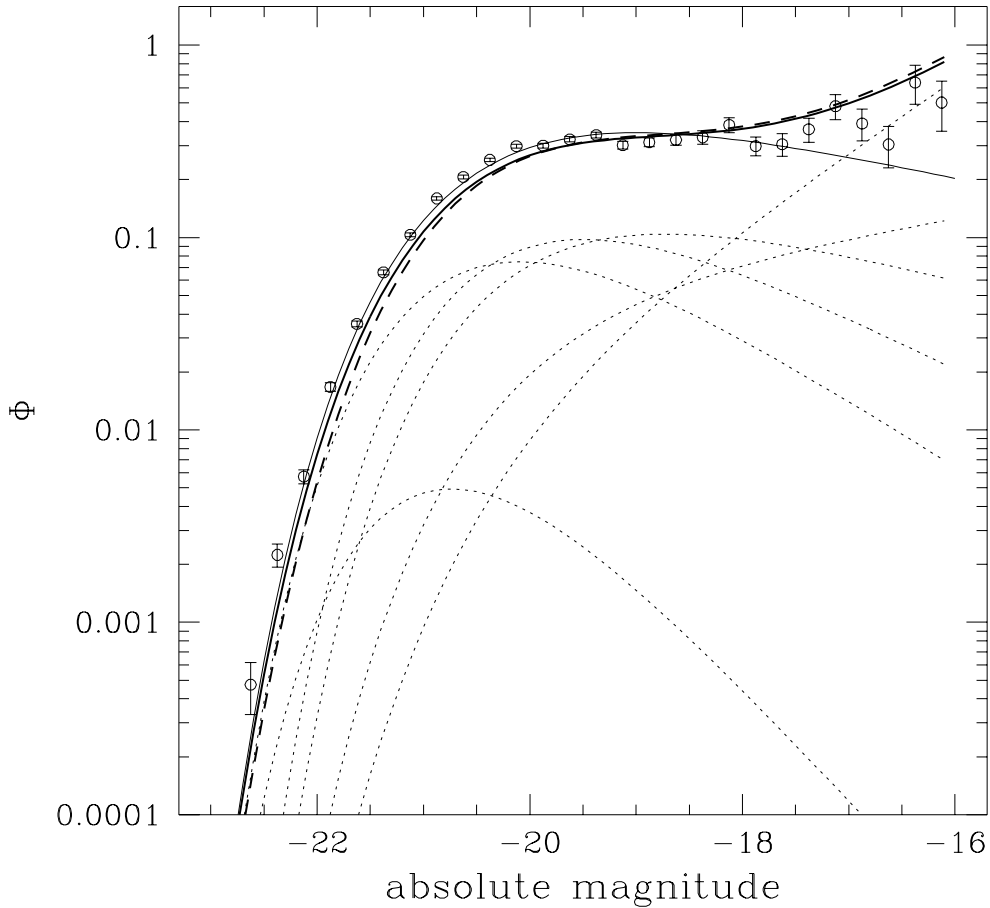


Fig. 7.— The general luminosity function. The points give the luminosity function from the nonparametric fit for the full, NS112 catalog, and the light solid curve is a Schechter function fit to the data. The heavy solid curve is the general luminosity function in equation (6), while the heavy dashed curve is the grand luminosity function (eqn. [13]). The individual clan luminosity functions which contribute to the general luminosity function are shown as well (light dotted lines); they are weighted according to their contribution. Note that the clan identity of the dotted curves can be easily determined from the faint-end slope (cf. Figure 5).

apparent. Probably the most leverage in generating a discrepancy between subsamples in a survey can be gained by changing the sampling rate of galaxies with low central surface brightness, m_c . For example, if we cut out all galaxies which have $m_c > 18$ mag, the faint-end slope becomes very shallow, with $\alpha = +0.06 \pm 0.04$. In contrast, the excluded low-surface-brightness galaxies has a faint-end slope of $\alpha = -2.5 \pm 0.8$. Nonetheless it is argued in LC2 that the problem arises not from the faint galaxies but from the bright ones, which can modify α if the Schechter parameterization gives only an approximate fit. Another possible source of the discrepancy is cosmic variance from large-scale structure and environmental effects. We proceed into this topic next, but we must bear the north-south differences in mind.

(Incidentally, if we divide the survey according to right ascension instead of declination, generating eastern and western subsamples, the discrepancy vanishes, mostly through a broadening of the error ellipsoids.)

4.3 Environmental dependence

We have thus far treated the general luminosity function (eq. [6]) under the assumption that the clan luminosity functions are each universal. Calculations of the general luminosity function for unrepresentative regions of the Universe (e.g., “the field” or in clusters) then can proceed simply from estimates of the local fraction of each galaxy type. However, it may be the case that type-specific luminosity functions are themselves dependent on density. We now test this possibility.

The LCRS population may be divided into low- and high-density subsets using the 3-dimensional redshift-space information. Of the many possible ways of making this division we opt for a friends-of-friends algorithm (Huchra & Geller 1982) to identify groups of objects in redshift-space. The objective here is to simply but unambiguously determine high density regions. We do not weigh the advantages and disadvantages of this choice except to say that while the method may misclassify some galaxies in small, high-density groups, it handles redshift-space distortions—particularly “fingers of God”—very well. For this exercise we choose link parameters of 80 km/s in the plane of the sky and 500 km/s along the line of sight. The resulting grouped galaxies, with a 4-object minimum group size, constitute about one-third of the total survey, including the N50 and S50 samples. These objects are labeled as high density, while the ungrouped objects are considered low density. A crude estimate of the density threshold is approximately 1,000 times the mean. The fraction of 112-fiber members within each clan that are tagged as high-density environments is given in the last column of Table 1.

Figure 8 illustrates the dependence of the clan luminosity functions on density while Figure 9 gives the best-fit Schechter parameters. The early-type galaxies (clans 1–3), accounting for over 70% of the objects in the survey, show significant variation: the faint-end slope steepens with density, with α shifting by about -0.5 . From the best-fit values of the Schechter parameters, we calculate that the mean luminosity of early-type clans in high-density regions is approximately 50–80% less than in the low-density regions. The late-type objects show little or no significant trend. This result is fairly insensitive to the north-south discrepancy noted above and may perhaps provide an explanation for it: Differences in the fraction of galaxies in high-density regions can alter the inferred universal luminosity functions in the southern sample relative to that of the north.

Note that the steepening of the luminosity function with increasing density occurs simultaneously with a change in the local fraction of types as described by the morphology-density relation (Dressler 1980; Postman & Geller 1984). We can take both effects into account, writing a more general form than in equation (6), call it the grand luminosity function,

$$\Phi_G(M) = \sum_{c,d} f_{cd} \Phi_{cd}(M) , \quad (13)$$

where the fraction of galaxies f and the clan luminosity functions both acquire a density index (here it can be just one bit). An estimate of this function shows that it is not significantly different from the general luminosity function for the NS112 sample. Thus for the purposes of understanding the global properties of a catalog, the general luminosity function is a reasonable approximation, as suggested by Binggeli et al. (1988). But the effect of environment is certainly important in the context of galaxy formation theories.

The dependence of the faint-end steepness on density, call it the α -density relation, suggests that, on average, galaxies of a given type are fainter in dense regions than in the field. This behavior is qualitatively consistent with the observation that the dwarf-to-giant ratio of early type galaxies is higher in groups than in the field (Ferguson & Sandage 1991). However, from a theoretical standpoint, this is an unexpected result.

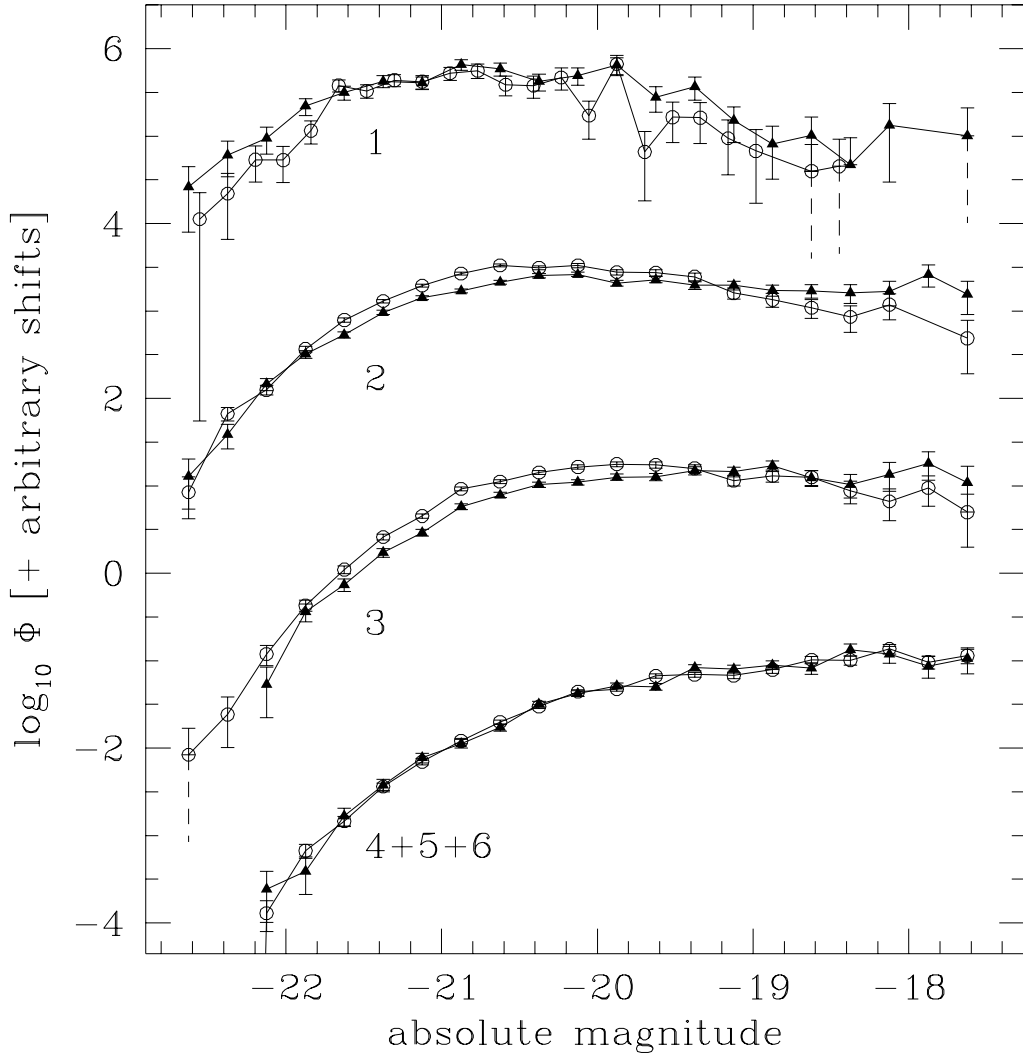


Fig. 8.—The luminosity function by clan and density. Nonparametric fits are shown, as in Figure 5, for objects in high-density regions (dark triangles) and low-density regions (open circles). The labels indicate clan index; the lower curves were produced by merging samples of the three late-type clans. The excess numbers of faint, early-type galaxies in the high-density cases are evident from the relative flatness of the luminosity functions above a magnitude of -20. The effect is not significant for the late-type clans.

Press-Schechter theory predicts a relative decrease in low-mass objects in overdense regions, as a result of a steeper decline of power with scale. One might assume that this prediction applies to galaxies of a single type and therein lies the unexpectedness of the α -density relation.

It may be that the Press-Schechter prediction is more suggestive of the change in the mix of galaxy types with density as opposed to the dependence of intrinsic properties of any one galaxy type. Thus, to understand any sort of α -density relation, one may have to identify the processes which determine a galaxy's type. Whatever these processes, the LCRS data suggest that they allow galaxies of a specific type to form with less mass in dense regions than in the field. Toy models which show this behavior may be easy to construct, but it may be more challenging to identify such an effect in more developed theories of structure formation or numerical simulations.

Alternatively, the α -density relation may not reflect anything special about galaxy formation but may indicate some mechanism that diminishes the luminosity of “mature” galaxies in dense regions. Tidal stripping comes to mind, but then one expects that the fainter late-type galaxies would be affected more than the brighter—and presumably more massive—early types. This is not observed in the LCRS data. There are ways out, of course, for example by invoking a scenario wherein only early-type galaxies get deep enough into cluster potentials to experience tidal stripping. In any event, the α -density relation should provide an interesting constraint for galaxy formation models.

4.4 Comparison with other catalogs

We now compare the luminosity function of the LCRS galaxies with those measured in other surveys. In type-independent analyses, there are clear discrepancies between the LCRS and other redshift surveys, with most of the differences attributed to faint magnitudes. The faint-end slope of the universal luminosity function is -0.7 ± 0.1 for the LCRS galaxies (LC2), considerably lower than has been estimated from optically selected surveys. For example, Loveday et al. (1992) find $\alpha = -0.97 \pm 0.15$ in the Stromlo-APM Redshift Survey, while the CfA redshift survey—containing over 10,000 objects selected on the basis of the Zwicky magnitude scale—has a faint-end slope of $\alpha = -1.0 \pm 0.2$ (Marzke, Huchra & Geller 1994).

As noted in LC2 there are a number of possible causes for the discrepancies. First, the choice of waveband can affect the mix of galaxy types in a survey, and hence the weight factors associated with the individual type-specific luminosity functions (eq. [6]). A second culprit may be the Schechter parameterization used to calculate the faint-end slope. In the LCRS survey we identified a broad shoulder in the general luminosity function at $M \approx -20$ and a faint-end slope which is evidently increasing with decreasing brightness. These features represent deviations from the Schechter form, and attempts to fit the universal luminosity function may well reflect the range of absolute magnitudes used in the analysis more than any intrinsic property of a galaxy population.

We must be cautious when considering the more recent results from the Century Survey (Geller et al. 1997) because the galaxies are selected with a red-band magnitude system very similar to that used in the LCRS. Yet the reported faint-end slope is $\alpha = -1.17 \pm 0.19$, consistent with the optically-selected data and well below the LCRS value. Geller et al. suggest that the central surface-brightness cuts in the LCRS bias the catalog toward high α values, i.e., more shallow faint-end slopes. The cuts account for no more than 7% of the total population, nonetheless, the known correlation between absolute magnitude and central surface brightness may produce a significant bias. We can estimate the importance of the effect by over-counting the clan-6 galaxies, with a very steep faint-end slope of -1.93 , so that they represent an additional 7% of the total population in the estimation of the Schechter parameters. The result shows that the inferred α value does steepen to -0.88 , but the luminosity function above $M = -17.5$ rises even more steeply, an effect not seen in the Century survey data.

While we do not rule out the central surface brightness cuts—the “missing” faint galaxies—as a source of the discrepancy between LCRS and the Century Survey, it is probably not the dominant effect. The reason is that the discrepancy comes not from the faint end of the luminosity functions but from the bright end: As noted in LC2, the Schechter parameter α is still highly sensitive to very bright objects in the range of absolute magnitudes used in both the LCRS and Century Survey analyses. To illustrate, we fit Schechter functions using a range with the bright-end absolute magnitude M_{bri} on the faint side of $M = -23$, the limit adopted by in LC2. The inferred α steadily decreased with increasing M_{bri} so that, at $M_{\text{bri}} = -21$, we found a best fit α of -0.85 , within the 2σ limits of the Century Survey result. Thus part of the problem in the comparing the two surveys is the failure of the Schechter parameterization, or more fairly, the interpretation of the fitted Schechter functions: a smaller (more negative) fitted value of α does not necessarily imply a

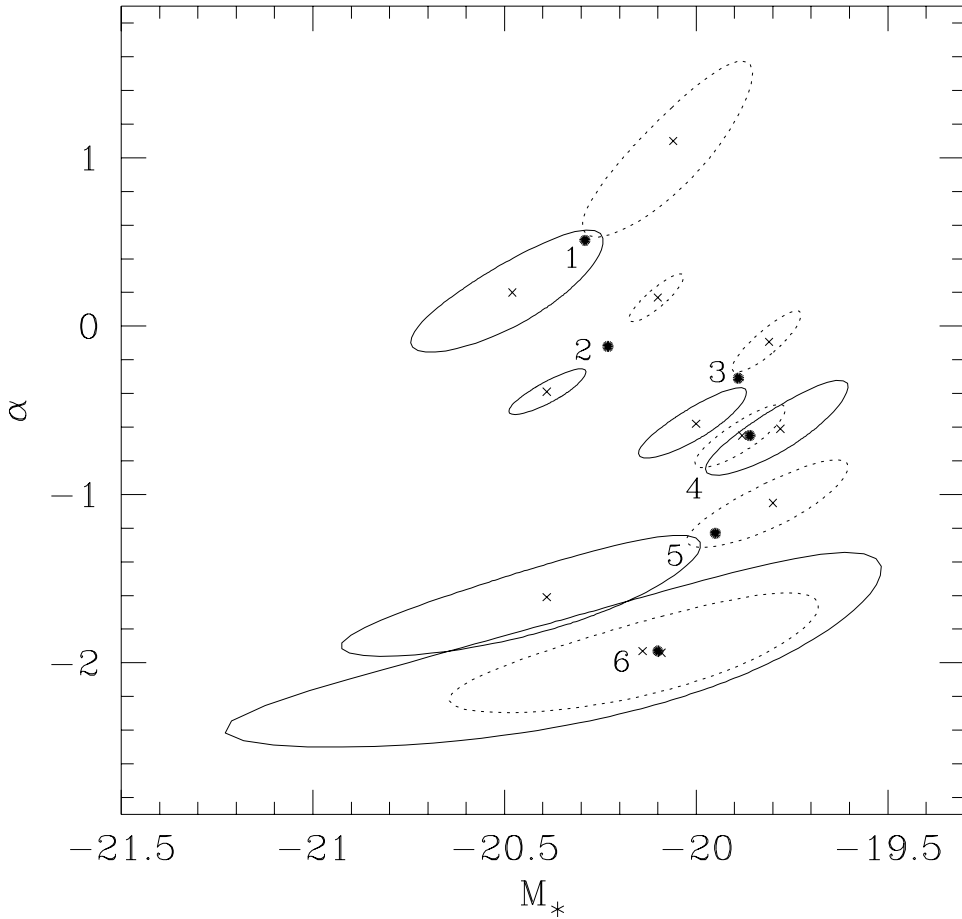


Fig. 9.—Error ellipsoids for the best-fit Schechter parameters for objects in high and low density regions. The labels indicate clan index, the best-fit values are marked with an \times symbol, and the ellipsoids show 95% confidence intervals for objects found in high-density regions (solid contours) and low-density regions (dashed contours). There is a significant shift in both M_* and α for some objects, particularly those of clan 2, as a result of local density. The downward translation of α values indicates a relative excess in the number of faint galaxies in the high-density cases. The shift of M_* toward greater brightness with increasing density is partly a compensating reaction of the Schechter-parameterization fit to keep the extreme bright end of the luminosity function approximately unchanged.

steeper faint-end slope. Indeed, visual inspection of the nonparametric estimates (Figure 7 here and Figure 2 in Geller et al.) shows that, if anything, the faint-end of the LCRS luminosity function has a *steeper* rise with decreasing brightness than that of the Century Survey.

We thus argue that the universal luminosity functions of the LCRS and Century Survey exhibit differences, but that the dissimilarities are not attributed to a shallower faint-end rise in the LCRS case. Instead the differences may involve the dependence of the luminosity function on local environment as discussed above in §4.3. The Century Survey encompasses the Corona Borealis supercluster, and it is possible that the early-type galaxies therein are not only more numerous but yield α values which are steeper than in a more representative volume of the Universe. Together, these effects could account for the fact that the Century survey yields a high α value relative to the LCRS, yet it does not show a marked steep rise at the faintest magnitudes (above $M_R = -17.5$) from the contribution of late-type objects.

This explanation of the differences between the LCRS and Century Survey results is marginally supported by an analysis of the Norris Survey of the Corona Borealis Supercluster (Small, Sargent & Hamilton 1997). The universal r -band luminosity function estimated for 236 field galaxies—chosen to be outside of the supercluster by means of a redshift cut—is in agreement with the LCRS results. While this may suggest that the differences between the LCRS and the Century Survey results lie in the presence of the supercluster in the latter case, it should be emphasized that the Norris sample is small and uncertainties in the estimated luminosity function are large (cf. Small, Sargent & Hamilton 1997, Fig. 5 therein).

A better comparison to the LCRS results will be enabled with the forthcoming type-dependent analysis of the Century Survey (Kurtz & Mink 1997). Meanwhile, other type-dependent studies have been limited to optically-selected surveys. For example, Loveday et al. (1992) analyze type dependence of the luminosity function in the Stromlo-APM Redshift Survey and Marzke et al. (1994) perform a similar analysis on the CfA Redshift Survey. Loveday et al. find a nearly flat faint-end slope ($\alpha = +0.2 \pm 0.35$) consistent with the early-type clans derived here, and a steeper slope ($\alpha = -0.8 \pm 0.2$) for late type galaxies, similar to late-type clans 3 and 4. Marzke et al. find generally steeper faint-end slopes with $\alpha = -1.87$ for their late-type objects (no errorbars are given). Furthermore, while the early-type objects tend to have shallower faint-end slopes, they do not require it—the luminosity functions of the early- and late-type galaxies were found to be indistinguishable. Without entering the fray as to the source of the conflicting CfA and Stromlo-APM results, we simply note a strong statistical significance of the trend seen in both optically-selected datasets that the faint-end slope tends to steepen in the progression from early to late type.

5 Conclusion

In this paper we have implemented a spectral classification scheme based on singular-value decomposition. The SVD approach isolates the most significant variations in the spectra of a catalog with a set of orthonormal basis vectors, or eigenspectra. Projection of individual galaxy spectra onto the most significant eigenspectra yields coefficients from which galaxy types can be determined. The method was applied to the Las Campanas Redshift Survey, and in that catalog we defined 6 spectral classes (here called clans). The physical properties of each clan were interpreted in terms of star formation; the known correlation between star-forming galaxies and morphological type (Kennicutt 1992) suggests that the clan index runs smoothly from early to late types.

A slight modification of this classification scheme allowed us to isolate a distinct population of objects which we identify as Seyfert 1 galaxies (0.6% of the total).

We then used the spectral types to study the luminosity function of galaxies. A strong type-dependence is identified, particular in regard to the faint-end slope, with α ranging from about +0.5 (early types) to -1.9 (late types). We include this type-dependence in the calculation of the general luminosity function and we identify a steeper faint-end slope than in a type-independent analysis. The general luminosity function exhibits a broad shoulder at an absolute magnitude of roughly -20 in the R -band, a significant deviation from the Schechter parameterization. Thus the specific mix of galaxy types is important and should be included in estimates of the general luminosity function.

We also examined the effect of local environment on the luminosity function and found a shift in the faint-end slope for early-type objects that depends on density. This result is a detection of significant differences in the luminosity functions of field and cluster galaxies. Qualitatively, the effect is to steepen the faint-end of the luminosity function with increasing density. This increase in the relative number of faint galaxies in high density regions may arise as a result of density-dependent galaxy formation or some process such as tidal stripping which lessens the luminosity of individual galaxies in high-density regions after the galaxies

have formed. Simple considerations of both possibilities do not yield strong support for either one. The effect may pose a nice challenge for theories of galaxy formation and evolution.

Finally we compared the LCRS luminosity function with those of other redshift surveys. Deviations from the Schechter parameterization, the mix of galaxy types, and the density of structures in each survey can all affect the inferred universal luminosity function. Comparison of the LCRS to the red-selected Century Survey (Geller et al. 1997) shows that the main differences do not lie at faint magnitudes but in the bright regime. It is at these brighter magnitudes where the luminosity function of early-type galaxies show marked dependence on density. Thus the smaller effective volume and the presence of the Corona Borealis supercluster in the Century Survey could induce significant changes in the luminosity function relative to that which is typical of the universe at large. Consideration of these factors may well resolve the differences between the LCRS data, the Century Survey, and other optically-selected catalogs.

The success of the spectral classification method used here on the LCRS galaxies suggests that it may be fruitfully applied to larger catalogs such as the upcoming Sloan Digital Sky Survey. Then, with better sky coverage we may be able to examine in greater detail the luminosity function, a critical ingredient for understanding cosmic structure formation.

We thank M. Kurtz for helpful discussions regarding spectral classification. WHP and BCB acknowledge funding from NSF Grant PHY 95-07695. BCB is grateful to NASA Offices of Space Sciences, Aeronautics, and Mission to Planet Earth for providing computing resources.

REFERENCES

- Allen, D. A., Norris, R. P., Meadows, V. S., & Roche, P. F. 1991, MNRAS, 248, 528
 Baldwin, J. A., Phillips, M. M., & Terlevich, R. 1981, PASP, 93, 5
 Bershady, M. A. 1995, AJ, 109, 87
 Binggeli, B., Sandage, A., Tamman, G. A. 1988, ARAA, 509
 Connolly, A. J., Szalay, A. S., Bershady, M. A., Kinney, A. L., & Calzetti, D. 1995, AJ, 110, 1071
 Dressler, A. 1980, ApJ, 236, 351
 Efstathiou, G., Ellis, R. S., & Peterson, B. A. 1988, MNRAS, 232, 431
 Ferguson, H. C., & Sandage, A. 1991, AJ, 101, 765
 Folkes, S. R., Lahav, O., & Maddox, S. J. 1996, MNRAS, 283, 651
 Geller, M. J., et al. 1997, AJ, in press.
 Holmberg, E. 1958, Medd. Lund Astron. Obs., Ser. 2, No. 128
 Huchra, J. P., & Geller, M. J. 1982, ApJ, 257, 423
 Kendall, M. G. 1975, Multivariate Analysis (London: Griffin)
 Kennicutt, R. C., Jr. 1992a, ApJ, 388, 310
 Kennicutt, R. C., Jr. 1992b, ApJS, 79, 255
 Kurtz, M. J., & Mink, D. J. 1997, in preparation.
 Lin, H., Kirshner, R. P., Shectman, S. A., Landy, S. D., Oemler, A., Tucker, D. L., & Schechter, P. L. 1996, ApJ, 464, 60 (LC2)
 Loveday, J., Peterson, B. A., Efstathiou, G., & Maddox, S. J. 1992, ApJ, 390, 338
 Marzke, R. O., Geller, M. J., & Huchra, J. P. 1994, ApJ, 428, 43
 Marzke, R. O., Geller, M. J., Huchra, J. P. & Corwin, H. G. 1994, AJ, 108, 437
 Marzke, R. O., Geller, M. J., Da Costa, L. N., & Huchra, J. P. 1995, AJ, 110, 477
 Morgan, W. W., & Mayall, N. V. 1957, PASP, 69, 291
 Odewahn, S. C., Windhorst, R. A., Driver, S. P., & Keel, W. C. 1996, ApJ, 472, L13
 Postman, M., & Geller, M. J. 1984, ApJ, 281, 95
 Press, W. H., Teukolsky, S. A., Vetterling, W. T., & Flannery, B. P. 1992, *Numerical Recipes* (Cambridge: Cambridge University)
 Sandage, A., Tamman, G. A., & Yahil, A. 1979, ApJ, 232, 352

- Shectman, S. A., Landy, S. D., Oemler, A., Tucker D. L., Lin, H., Kirshner, R. P., and Schechter, P. L. 1996, *ApJ*, 470, 172 (LC1)
- Small, T. A., Sargent, W. L. W., & Hamilton, D. 1997, *ApJ*, 487, 512
- Roberts, M. S., & Haynes, M. P. 1994, *ARA&A*, 32, 115
- Zaritsky, D., Zabludoff, A. I., & Willick J. A. 1995, *AJ*, 110, 1602